# *Ab initio* study of evolution of mechanical and transport properties of clean and contaminated Au nanowires along the deformation path

Pavel Jelínek,[1] Rubén Pérez,[2] José Ortega,[2] and Fernando Flores[2]
[1]*Institute of Physics, Academy of Sciences of the Czech Republic, Cukrovarnická 10, 162 53 Prague, Czech Republic*
[2]*Departamento de Física Teórica de la Materia Condensada, Universidad Autónoma de Madrid, Madrid E-28049, Spain*
(Received 5 July 2007; revised manuscript received 23 November 2007; published 25 March 2008)

We present a first-principles study of the evolution of the mechanical and transport properties of clean and contaminated Au nanowires during the whole breaking process. We combine density functional theory total energy calculations and Keldysh Green's function methods in order to determine the changes in the structure and conductance induced by the presence of hydrogen and oxygen atomic impurities. Our simulations show how atomic oxygen is incorporated into the nanowire, forming long monoatomic chains, in good agreement with the experimental observation. The presence of adsorbed atomic impurities introduces significant changes in the conductance, providing a quantitative explanation for the new peaks found in the conductance histograms recorded in the presence of the corresponding molecular species. The exothermic character of the dissociation process in the nanowire found in our study provides a sound basis for the presence of these atomic impurities, although the problem of finding a low-activation energy path for the oxygen molecule remains open. This enhanced chemical reactivity can be traced back, through the analysis of the local density of states, to both the reduced coordination and the applied tensile strain.

DOI: 10.1103/PhysRevB.77.115447 PACS number(s): 73.63.−b, 68.43.Bc, 62.25.−g, 73.63.Rt

## I. INTRODUCTION

The electrical and mechanical properties of metallic nanowires have been under intensive experimental and theoretical investigation[1] in the past years. In particular, the gentle control of the distance between two metals achieved by scanning tunneling microscopy–atomic force microscopy or a mechanically controlled breaking junction (MCBJ)[3] has allowed the experimental characterization of atomic contacts and the observation of quantum effects in both the conductance and the forces.[2] In a pioneering work, Scheer *et al.*[4] have unveiled, from an analysis of the superconducting properties of an atomic contact, the relation between the chemical valence and the electrical resistance of the system just before the breaking point. These experiments showed that each atomic contact can be uniquely characterized in terms of the number of channels and their transmission probabilities contributing to the conductance.

Further understanding of the mechanical and electrical properties of different nanocontacts has been achieved by the simultaneous experimental characterization of the conductance and tensile forces along the stretching process.[5] The measurements showed how conductance and force jumps take place at the same stages, being related to the irreversible (plastic) deformation of the nanowires to new stable structures. On other hand, conductance histograms, where the values of the conductance for thousands of different contacts are collected, provide further evidence of the role of the nanowire geometry in the determination of the mechanical and electrical properties: The peaks in the histogram reflect the stable atomic configurations of the junction before breaking.

From a theoretical point of view, the understanding of these quantum effects in the force and the conductance along the stretching path is not an easy task, requiring three different key ingredients: the detailed knowledge of the nanocontact structure, a quantum mechanical calculation of the electronic properties associated with this geometry, and an accurate description of intrinsically nonequilibrium phenomena such as electronic transport. The formation of necks and atomic contacts in stretched metallic nanowires has been analyzed theoretically using different approaches. The first studies of the nanowire formation were based on molecular dynamics simulations using either classical[6,7] or effective-medium theory potentials.[8,9] Predictive *ab initio* methods based on density functional theory (DFT) provide a reliable description of the electronic structure and the mechanical stability of the nanocontact. However, the large computational cost has restricted most of the applications (apart from Alkali metal nanowires,[10] thanks to their particularly simple electronic structure) to the static analysis of model geometries for the contact (e.g., single-atom or short atomic chains in between pyramids or planes with the given nanocontact orientation).[11–17] This approach has failed to reproduce basic experimental features of nanocontacts close to the final breaking stage, such as the characteristic increase in the conductance upon stretching in Al or the value close to the conductance quantum $G_0=\frac{2e^2}{h}$ found systematically in the experiments irrespective of the orientation or initial conditions [for example, the theoretical conductance of a single-atom contact between two (100) Al pyramids is $3G_0$ (Ref. 17)].

These discrepancies between theory and experiment prompted our recent large-scale simulations of the evolution of different Al nanowires (including up to 145 atoms)[18–20] under tensile stress along the whole elongation process. Our goal was to assess the influence of size and crystallographic orientation and the role of defects (impurities such as O, H, and C)[20] in the structure, mechanical response, and conductance in the final stages of nanowire deformation. Our approach combined a very efficient local-orbital pseudopotential DFT approach [FIREBALL (Refs. 21 and 22)], which gave direct access to a realistic structure of the nanocontact, with a consistent and accurate determination of the transport prop-

 

erties based on the Keldysh Green's function formalism (see Refs. 19 and 23). These simulations have provided a comprehensive picture of the plastic deformation of Al nanowires approaching their breaking point, where, irrespective of the initial configuration and orientation, all of them evolve to the same final dimer geometry that is responsible for the common conductance properties found before the breaking point in the experiments. In particular, we were able to reproduce the ascending shape of the last plateau in Al nanocontacts. Impurities do affect the mechanical response of the nanocontact but do not modify the final dimer geometry and the associated conductance properties.

While for most metals the nanocontact structure just before the breaking point is characterized by an atomic dimer geometry, experiments have convincingly proven the formation of single-atom chains (including up to seven or eight atoms) between the two electrodes for 5*d* metals such as Au, Pt, and Ir.[24] The electronic and vibrational properties of these nanowires have been characterized in detail experimentally, particularly for Au. The possible role of impurities in the structural and electronic properties of the gold atomic chains has been studied intensively.[25–32] The original motivation came from the anomalously large interatomic distances ($\approx$4 Å) observed in high resolution transmission electron microscopy (HRTEM) measurements[33] on suspended gold chains at room temperature and under ultrahigh vacuum (UHV) conditions. These large Au-Au distances were in contradiction with early theoretical studies on the formation and stability of pure monoatomic Au chains.[34–36]

The suggested explanation, supported by total energy calculations and molecular dynamics (MD) simulations,[25–32] involves the accidental incorporation of light atomic contaminants (such as H,C,O, and S), which are always present in the UHV chamber but, in principle, cannot be imaged by HRTEM. The most recent MD simulations,[32] performed at $T \approx 600$ K, suggest sulfur as the most likely contaminant. Notice that these conditions (small concentration of the atomic species acting as impurities and very high temperatures) are completely different from the cryogenic measurements with intentional contamination in the UHV chamber up to 20 K, which we discuss below.

MCBJ experiments under cryogenic vacuum conditions[37] seem to be free of that contamination problem, as they provide values for the Au-Au distances in the chain around 2.5 Å, similar to the ones found in *ab initio* calculations. Therefore, they are the perfect playground to address, *by intentional contamination with molecular species such as* $H_2$ *and* $O_2$, the chemical reactivity of these one dimensional (1D) systems and the role of impurity atoms on the formation of metallic nanocontacts and their mechanical and transport properties. Csonka *et al.*[38,39] have analyzed the interaction of molecular hydrogen with a breaking gold nanowire and have found new fractional peaks (in units of the conductance quantum $G_o = \frac{2e^2}{h}$) in the conductance histogram. Moreover, conductance traces in a stretched nanowire demonstrate a reversible transition between fractional and integer conductances in a time scale of milliseconds or seconds, suggesting successive adsorption and desorption of hydrogen on the chain. This effect has not been observed in similar experiments for Cu and Ag where stable monoatomic chains are not formed. This points out the crucial role of the Au chains in the variation of gold conductance in the presence of $H_2$. Recently, a similar MCBJ experiment[40] reports the formation of atomic chains for gold and silver, which is strongly enhanced admitting $O_2$ in the UHV chamber. The experimental data strongly suggest the incorporation of oxygen atoms in the Au and Ag chains, reinforcing the metallic bonds.

Some of these issues, including reactivity and the possible incorporation of atomic or molecular species into the chain, have been studied before by DFT calculations.[25–32] Bahn *et al.*[26] have predicted the strong chemical activity of the ideal infinite single-atomic Au chains, leading to the incorporation of atomic oxygen and the formation of energetically stable gold-oxygen chains. Barnett *et al.*[29] have studied the chemical reactivity of a more realistic system: an ideal monoatomic gold chain sandwiched between two Au tips. Their calculations point out that the enhanced chemical reactivity of gold nanowires induces a "molecular welding," the process where a hydrogen molecule $H_2$ incorporates into a broken Au wire and restores the ballistic transport through it. The same highly symmetric model, including a monoatomic Au chain between two identical contacts simulated by 20-atom tips, has been considered in the most recent DFT calculations addressing the incorporation of H and C atoms.[31]

In this paper, we take advantage of the efficiency of our DFT–local density approximation (LDA) local-orbital basis approach in order to go beyond those simple models and to study the interaction of atomic and molecular hydrogen and oxygen with realistic nanowire structures, which include single-atom Au chains of different lengths, and the contacts with the electrodes, which have been obtained through a complete simulation of the stretching process of thicker wires up to the final breaking point. In this way, we can characterize the reactivity at the different stages of the breaking process and even study the influence of the impurity in the nanowire formation process, including it in the simulations of the stretching process, in order to understand the enhanced atomic chain formation in the presence of molecular oxygen found in the experiments.[40] The coupling of our local-orbital basis approach with Keldysh Green's function methods makes it possible to correlate the changes in structure and mechanical strength in the wire with the evolution of the conductance, the key quantity that it is directly accessible to the experiments and that was not addressed in previous studies. This combined approach to the mechanical and transport properties was the basis for our recent study of the origin of the fractional conductance peaks observed in Au nanocontacts in the presence of molecular hydrogen, which we attributed to the dissociation of the $H_2$ molecule in the highly reactive chains.[41] Here, we further substantiated the reactivity of these systems due to both the reduced dimensionality and the tensile strain, with a detailed analysis of the local density of states (LDOS) of the Au nanowire along the stretching path and the influence on the LDOS of the atomic impurities, including the oxygen case. The main goal of our work is to show the direct relation between these LDOS characteristics and both the enhanced reactivity and the changes in the conductance.

The rest of the paper is organized as follows. In Sec. II, we summarize our theoretical approach for the calculation of

the atomic relaxations induced by the stretching process and the corresponding electronic transport properties. Section III is devoted to the description of the structural evolution of a pure gold contact along the stretching paths. The interaction of molecular and atomic hydrogen with gold atomic chains is analyzed in Sec. IV, with particular emphasis on the interplay between the electronic structure and the reactivity. In Sec. V, we discuss the formation of single-atom gold chains in the presence of atomic oxygen during the stretching path. Besides the description of the process leading to the incorporation of these species into the chain, we calculate the corresponding evolution of the transport properties. The comparison of these theoretical results with the experiments suggests that $O_2$ dissociation takes place in the Au chain. Therefore, we explore the feasibility of this process with a more accurate plane-wave code using the generalized gradient approximation (GGA) exchange-correlation functional, studying the possible reaction paths on strained ideal 1D chains,as we did recently for the case on molecular hydrogen.[41] We conclude (Sec. VI) with a discussion of the behavior of the two different chemical species acting as impurities and with a comment on the general validity of our results.

## II. METHOD

Handling the complex deformation process of nanocontacts with a fully converged first-principles description is still too computationally demanding. One possible approach is to choose an accurate plane-wave (PW) DFT method and to carefully relax the conditions for convergence (basis set cutoff, *k*-point sampling, etc.) in order to make the calculation feasible.[42] A second, more convenient, alternative is to use local-orbital DFT methods, specially those devised with the aim of computational efficiency. The formulation in terms of local orbitals has an added value, as the transport properties can be easily calculated from the resulting (tight-binding or linear combination of atomic orbitals) electronic Hamiltonian using Keldysh Green's function techniques.[20,23] Thus, efficient local-orbital DFT methods are probably the best available tools for a first-principles analysis of complex nanowires. In this work, we have studied the evolution of the structure and the conductance of a Au nanocontact as a function of the tensile strain for the whole stretching process by means of a fast local-orbital basis DFT-LDA technique (FIREBALL).[21,22] This technique offers a very favorable accuracy/efficiency balance if the atomiclike basis set is chosen carefully.[43] In the present calculations, the valence electrons of Au were described by a basis set of *s*, *p*, and *d* slightly excited pseudoatomic orbitals[44] with cutoff radii $R_c(s)=4.5$ a.u., $R_c(p)=5.2$ a.u., and $R_c(d)=4.0$ a.u. This basis set provides a lattice parameter for fcc Au of $a=4.14$ Å and a bulk modulus of $B=210$ GPa (experiment: $a=4.07$ Å and $B=173$ GPa). In the case of hydrogen atoms, we used a double numerical *s*-orbital basis set with the following cutoff radii $R_c(s)=3.8$ a.u. Finally, O has been approximated by a double numerical basis set with cutoff radii $R_c(s)=3.4$ a.u. and $R_c(p)=3.8$ a.u.

In our simulations for the single-atom chain formation, we start with a structure defined by a neck of four layers, with three atoms in each layer, sandwiched between two (111)-oriented metal electrodes, as shown in Fig. 1(a). We use a supercell approach, where periodic boundary conditions along different directions are introduced: We have considered a $3\times3$ periodicity parallel to the surface, while in the perpendicular direction we join artificially the last layers of both electrodes (similar to Refs. 18 and 20). Thus, our unit cell contains 48 atoms. In order to determine the stable structures during the stretching process, the two external surface layers are rigidly displaced (keeping the atoms in the bulklike configuration) in order to simulate the external strain, while the rest of the atoms (30) are allowed to relax to their ground state configuration (zero force) for the given external conditions using a conjugated gradient method. Each geometry has been converged until energy changes and total forces on every atom are below $10^{-6}$ eV and 0.05 eV/Å. In this structural configuration, the Brillouin zone has been sampled by a mesh of $4\times4\times1$ ($8\times8\times1$) Monkhorst-Pack *k* points in the total energy (conductance) calculations. The use of just

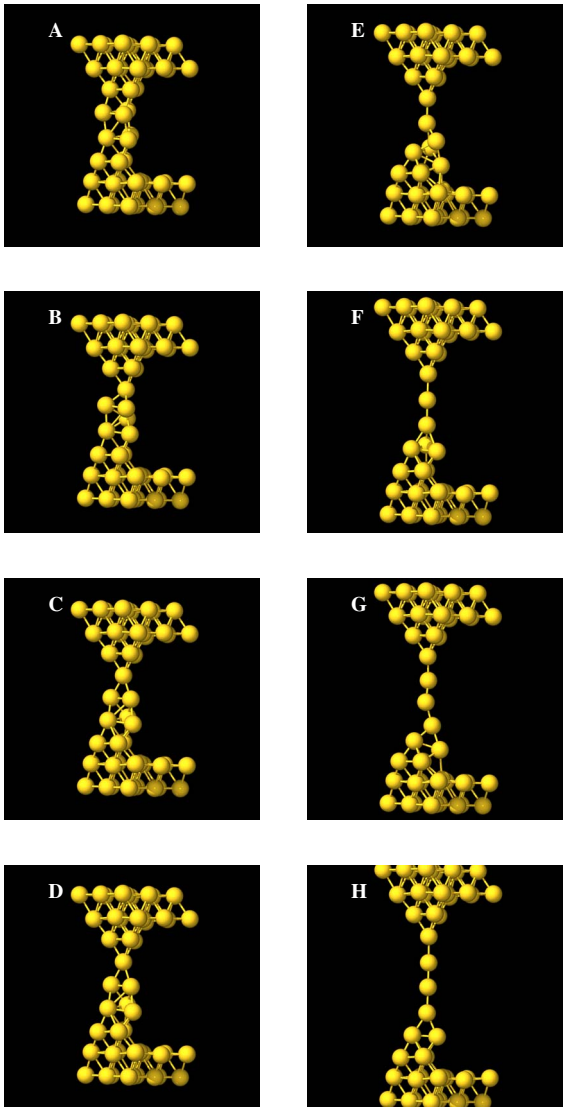


FIG. 1. (Color online) Ball-and-stick structure models for different snapshots of the simulation along the stretching path showing the formation of a clean gold monoatomic chain.

one $k$ point in the stretching direction is consistent with the aperiodic character of the real system in this direction. This approach is complemented with PW-DFT calculations with a gradient corrected approximation[45] (GGA) for the exchange-correlation functional [using CASTEP (Refs. 46 and 47)] for ideal infinite monoatomic chains in the presence of atomic and molecular impurities in order to provide an accurate assessment of the chemical reactivity and the dissociation paths for the hydrogen and oxygen molecules. In this particular case, the total energy calculations of the infinite 1D nanowire have been performed using four $k$ points in the wire direction. Although the real system considered with our fast DFT code is much more complicated than this freely suspended wire, this study will be indicative of the influence that a Au nanowire can have on the feasibility of this reaction by lowering the corresponding activation barriers. Furthermore, apart from capturing the key ingredients in the real nanocontact structure (determined with the fast local-orbital code), this simplified model provides a natural playground to explore the influence of the low dimensionality and the strain in the different steps of the dissociation process.

The electrical conductance of the nanowire is calculated using a Keldysh Green's function approach based on the first-principles tight-binding Hamiltonian corresponding to the relaxed structure obtained at each point of the deformation path. In our formalism, the total system is split into two subsystems, 1 and 2, and the total Hamiltonian is written as $\hat{H}=\hat{H}_1+\hat{H}_2+\hat{T}_{12}$, where $\hat{T}_{12}$ defines the coupling between both subsystems. Then, the differential conductance[23] can be written as

$$G=\frac{dI}{dV}=\frac{4\pi e^2}{\hbar}\mathrm{Tr}[\hat{T}_{12}\hat{\rho}_{22}(E_F)\hat{D}^r_{22}(E_F)\hat{T}_{21}\hat{\rho}_{11}(E_F)\hat{D}^a_{11}(E_F)] \tag{1}$$

where $\hat{\rho}_{11}$ and $\hat{\rho}_{22}$ are the density matrices associated with sides 1 and 2, respectively, while

$$\hat{D}^r_{22}=[\hat{1}-\hat{T}_{21}\hat{g}^r_{11}(E_F)\hat{T}_{12}\hat{g}^r_{22}(E_F)]^{-1} \tag{2}$$

and $\hat{D}^a_{11}$ is given by a similar equation; $\hat{g}^r_{11}$ and $\hat{g}^r_{22}$ are the retarded Green function of the decoupled sides, 2 and 1.

Similar approaches,[15–17,49,50] based on the combination of *ab initio* calculations on local-orbital basis and Green function methods, have been recently applied to characterize some ideal geometries (mainly, atomic chains) for Al and Au nanowires. The analysis of the different eigenchannels contributing to the differential conductance has been performed by diagonalization of the transfer matrix (for details, see Ref. 19).

## III. CLEAN Au NANOCONTACT

In this section, we describe the simulations for the breaking process of the *thick* 3×3 Au wire shown in Fig. 1(a) under tensile stress conditions and the formation of single-atom chains. In our calculations, the nanowire is stretched by increasing the distance between the last layers of the electrodes at each step by 0.2 Å (0.4 Å in the simulations with the oxygen impurity). Figure 2 shows the total energy of the system as a function of the stretching displacement with the characteristic jumps of the energy associated with the irreversible structural deformations. The system undergoes several atomic rearrangements along the deformation path, finally reaching a one-atom contact between points C and D (for details, see Fig. 1). Further stretching of this stable atomic configuration leads to the D→E jump, where a second Au atom is extracted from the electrode and incorporated into the chain. The next critical step takes place near point F, where, by a similar process, the wire develops a three-atom chain. Finally, after the G→H jump, the system shows a four-atom nanowire. Notice that after the incorporation of a new atom, a zigzag structure[51] is observed [see Fig. 1(g)]. Upon further loading, the chain straightens [see Fig. 1(h)] until a new atom is incorporated into the chain or the contact is finally broken. A substantial rearrangement of atoms in the neck, involving the formation of a small cluster near one of the electrodes, takes place at this final breaking step. In our simulation, the average length of a Au-Au bond of the zigzag structure is around 2.6 Å and the final chain length at the breaking point is ≃8 Å, with a Au-Au bond distance of ~2.9 Å. Similar results have been obtained using a parametrized tight-binding molecular dynamics calculation.[52]

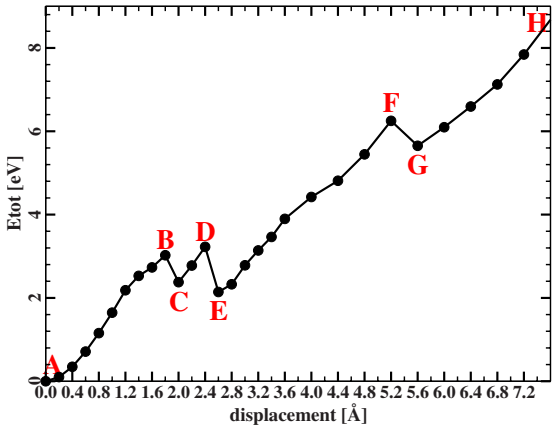


FIG. 2. (Color online) Total energy per unit cell of the clean Au nanowire as a function of the stretching displacement $\Delta d$. The energy of the initial relaxed configuration has been taken as a reference.

Figure 3 displays both the tensile forces, calculated as a numerical derivative of the total energy, and the conductance of the system along the stretching process. The characteristic oscillatory character of the force curve is associated with the cyclic character of the deformation process, incorporation of a new Au atom from the electrodes, leading to a chain formation. The continuous increase of the force corresponds to the steps where the system deforms elastically and accumulates internal stress, while the sudden reduction is associated with plastic events leading to a new bonding configuration where the internal stress has been released. In this case, the abrupt drop in the force is driven by the incorporation of a new atom into the chain. The forces that we calculate for the different incorporation stages leading to the atomic chain formation are around 3 nN. This value is larger than the 1.5–2 nN found in the experiments. This fact might be re-

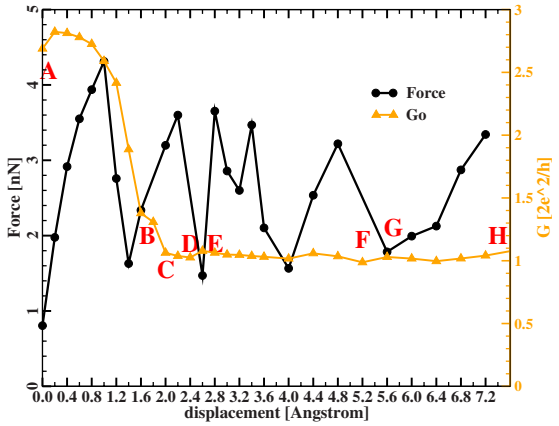


FIG. 3. (Color online) Total differential conductance and tensile forces along the stretching path (as in Fig. 2) for the case of a clean Au nanocontact.

lated to the elasticity of the real mesoscopic electrodes (not properly described with our model), and it is probably also influenced by the use of a restricted basis set in our calculations.

The conductance of the initial relaxed structure where the neck has three Au atoms per plane is close to $3G_0$, with $G_0$ being the conductance quantum $\frac{2e^2}{h}$. This value decreases continuously along the ABC deformation path (see Fig. 3), where the systems evolve toward a single-atom contact, finally reaching a value close to $G_0$. For the rest of the stretching process–C→H, where the single-atom chain is formed–the conductance shows the characteristic flat plateau with a value near $G_0$, with very small oscillations ($\leqslant 0.1G_0$) that correlate with the incorporation of new atoms into the chain. From the analysis of the eigenchannels contributing to the total conductance of the monoatomic chain, we have found one open channel mainly formed by the *s* orbital. At the final breaking step, the conductance drops to typical tunneling values close to zero, which confirm that the two contacts are effectively decoupled.

Note that our results match well with the experimental evidence.[2,5] In particular, we reproduce (a) the characteristic formation of Au monoatomic chains (with up to four atoms), (b) the long conductance plateau, with a value near $G_0$, associated with the presence of the monoatomic chain (configurations C→I), where the conductance is basically controlled by a single channel associated with the Au *s* electrons, and (c) the small conductance oscillations ($\sim 0.10-0.15G_0$) along the elongation process measured in most of the experiments.[2,5,53] Contrary to these measurements and to our results, large variations of the conductance depending on the strain and the number of atoms in the wire have been reported in a recent theoretical study.[54] Given the similarities in the theoretical approach (*ab initio* calculations for the electronic structure combined with a nonequilibrium Green's function method for the electronic transport), differences must be related to the different structures for the nanocontact. Grigoriev *et al.*[54] have considered a highly symmetric structure, where a monoatomic chain is inserted between two identical planar electrodes. This geometry departs radically from the results found in our calculation, where a rather asymmetric configuration for the contacts with the two electrodes is found. This mechanical asymmetry naturally appears during the process and reflects in the preferential incorporation of the atoms in the chain from only one of the electrodes. Symmetry is known to play a role in the conductance values since the early theoretical studies on the parity oscillations in monoatomic chains.[55] Sim *et al.*,[57] using first-principles calculations and exploiting the Friedel sum rule, found that the conductance for an odd number of atoms is equal to the quantum unit of conductance, independent of the geometry of the metallic banks, as long as they are symmetric for the left and right connections. On the other hand, the conductance is significantly smaller than $G_0$ and sensitive to the lead structure for an even number of atoms.

The absence of large conductance variations in the experiments seems to indicate that the real contacts are far from the ideal symmetric configurations considered in most of the calculations, where spurious interference effects can play a significant role. Notice, however, that the phase and size of the conductance oscillations also depend on the nature of the atoms involved, the crystallographic orientation, and the strain and shape of the electrodes.[56] All these considerations further stress the importance of an alternative approach, such as the simulation of the whole breaking process followed in our work, in order to get access to more realistic wire structures where all these factors are taken into account.

As we will discuss in the following section, the enhanced reactivity of these monoatomic chains and, thus, their ability to dissociate different molecular species play a crucial role in the understanding of the conductance changes found in the experiments. The role played by the lower coordination (compared to the surface or bulk structures) in these almost perfectly 1D structures can be understood through the analysis of the LDOS: the density of states projected in each individual atom. The top panel in Fig. 4 shows the LDOS for the four different atoms in the chain corresponding to the structure labeled G in Fig. 1. The significant changes in LDOS among the individual atoms according to their local atomic arrangement can be clearly observed. These changes are mainly manifested by the shift of *d* bands toward the Fermi level and their narrowing, with a width that is inversely proportional to the number of nearest neighbors. In particular, those atoms forming the monoatomic chain having only two nearest neighbors show very narrow *d* bands located less than 1 eV below the Fermi level. For atoms with a higher coordination, the LDOS converges rapidly to bulklike LDOS. The analysis of the LDOS evolution along the stretching path shows that the strain produces the same effects as the undercoordination, inducing further displacement toward the Fermi level and narrowing of the *d* bands. These two effects, the strain and the undercoordination associated with the 1D character of the Au chains, will prove to be crucial in making the dissociation of molecular species such as $H_2$ feasible.

## IV. INTERACTION OF ATOMIC AND MOLECULAR HYDROGEN WITH THE Au NANOCONTACTS

Here, we analyze the interaction of atomic and molecular hydrogen with the Au nanocontacts, paying particular atten-

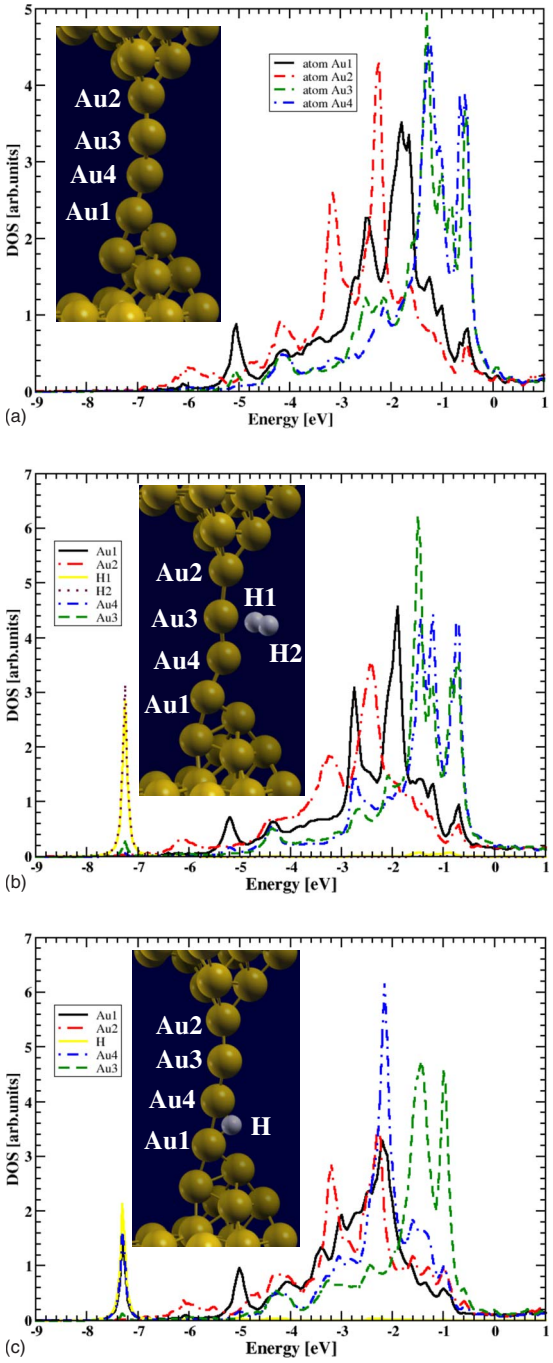


FIG. 4. (Color online) Local density of electronic states (LDOS) for different atoms in a clean Au monoatomic chain (upper panel), a Au nanowire with $H_2$ molecule (middle panel), and atomic *H* (lower panel).

tion to the modifications induced in the nanowire conductance at the different stages of the chain formation process. To that end, we have taken as a starting point the geometries labeled E, F, and G in Fig. 1, which correspond to chains including 2, 3, and 4 Au atoms, respectively. Then, we have studied the adsorption of one or two H atoms or a $H_2$ molecule located in different initial positions with respect to the Au nanowire. For each of these initial configurations, we have relaxed the system to its ground state configuration using FIREBALL, our DFT local-orbital basis code, with the

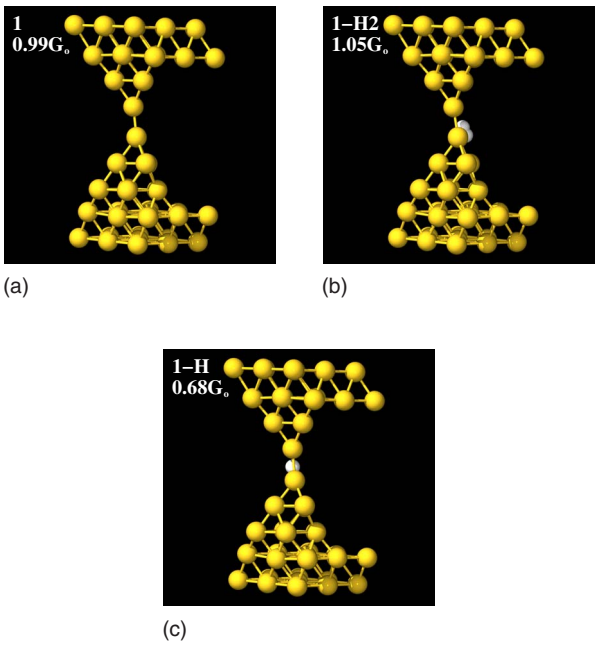


FIG. 5. (Color online) Ball-and-stick model of the relaxed atomic structures [corresponding to a stretching displacement of 2.8 Å, Fig. 1(e)] for the clean Au nanowire (left) and the wire contaminated with molecular (center) and atomic hydrogen (left).

LDA approximation for the exchange-correlation functional. Figures 5–7 display the relevant final structures we have obtained. The corresponding adsorption energies are listed in Table I. Notice that we are considering, for both the atomic and molecular species, the molecular adsorption energy $\delta E^{mol}=(E^{ads}-E^{clean})-0.5nE^{H_2}$, where $n$ is the number of hydrogen atoms. This definition, which takes as a reference the energy of the molecule calculated with our FIREBALL-LDA method ($E^{H_2}=-30.16$ eV), is particularly suitable to discuss the feasibility of the molecular dissociation and the exothermic character of the process.

The results in Table I show that the interaction of molecular hydrogen with all the different nanowires (structures labeled 1-H2, 2-H2, and 3-H2 and displayed in Figs. 5–7, respectively) is weak, leading to adsorption energies around 0.3 eV. None of these optimized structures support the penetration of molecular hydrogen into the nanowire. Actually, the presence of $H_2$ does not modify significantly the structural and electronic properties (see the discussion of the LDOS below) of the different chains, leaving both the Au-Au distance and the conductance practically unchanged. In particular, for the three cases 1-H2, 2-H2, and 3-H2, the nanowire conductance takes the values $1.05G_0$, $1.05G_0$, and $0.95G_0$, respectively.

On the contrary, the adsorption of atomic hydrogen introduces more dramatic changes. In particular, for a single hydrogen atom, the molecular adsorption energies $\delta E^{mol}$, with the FIREBALL-LDA method, are $\approx -0.3$, $-0.6$, and $-1.0$ eV for the Au chains including two, three, and four atoms, respectively (see Table I). These values, when compared to the +0.76 eV found for H adsorbed on the Au(111) surface (also calculated with FIREBALL-LDA), provide a clear indication of the much larger reactivity of the Au chains, where the

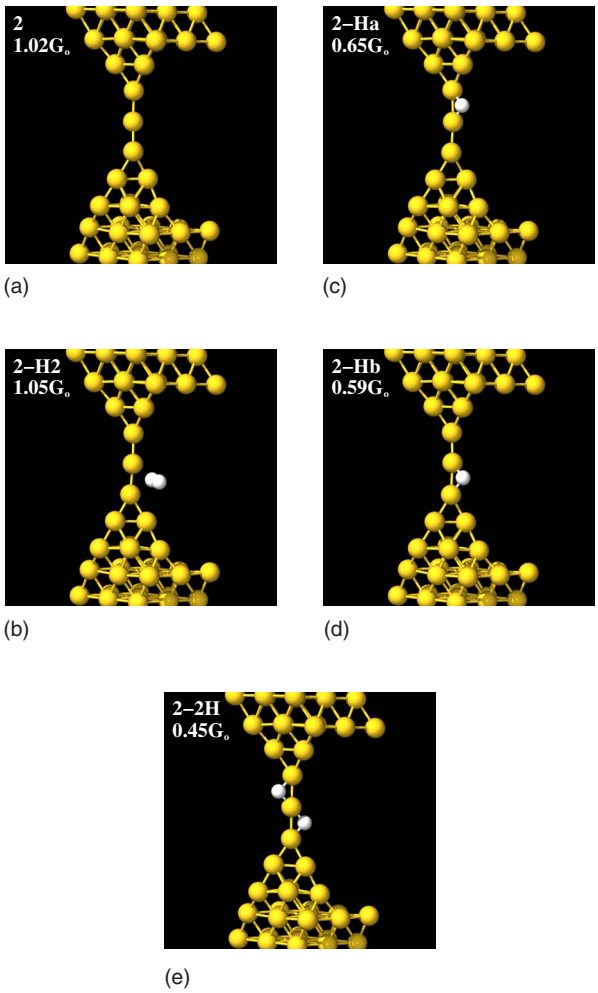


FIG. 6. (Color online) Same as Fig. 5 for a stretching displacement of 4.0 Å [corresponding to Fig. 1(f)]. The structures 2-Ha and 2-Hb correspond to two different initial locations for the atomic hydrogen, while 2-2H explores the influence of simultaneous adsorption of two H atoms on the short chain.

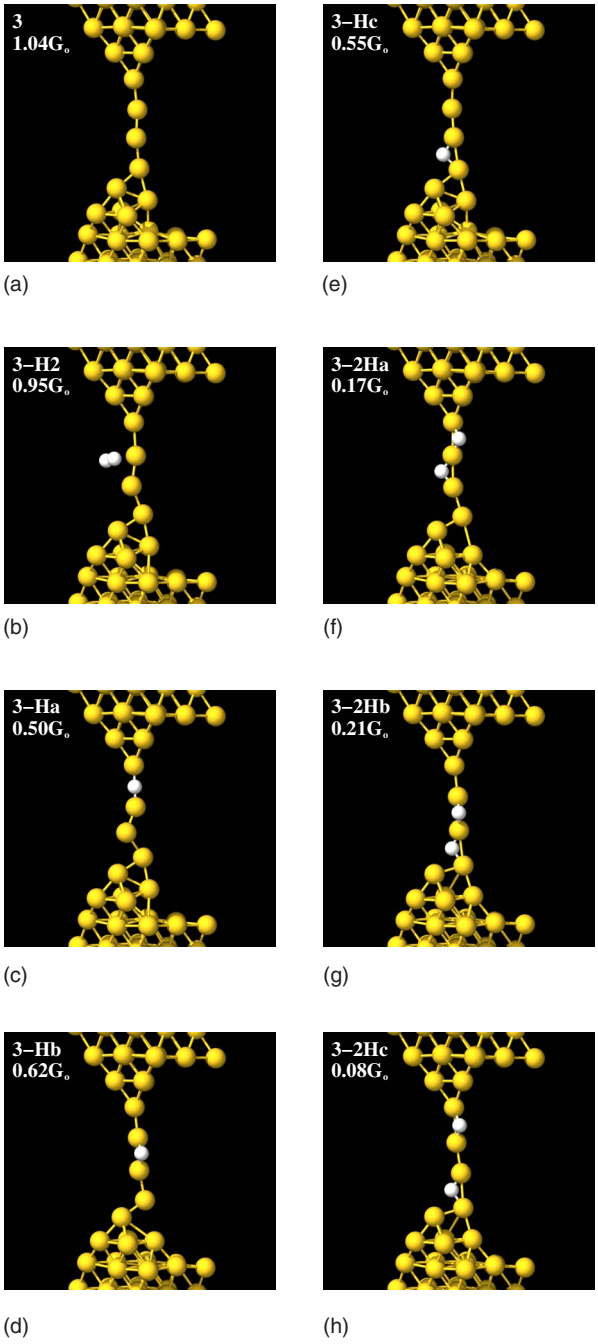


FIG. 7. (Color online) Same as Fig. 5 for a stretching displacement of 6.0 Å [corresponding to Fig. 1(g)].

strength of the interaction with H actually increases with the length of the chain. The Au-Au bond distance between the gold atoms directly bonded with atomic hydrogen is increased by 0.1 Å. Further support for this strong interaction comes from the significant modifications found in the conductivity for the three chain lengths, with total values of $0.68G_0$, $0.65G_0$, and $0.55G_0$, for the two-, three- and four-atom chains, respectively. In addition, we have also considered the simultaneous adsorption of two hydrogen atoms on the chains with three or four Au atoms as a likely product of the dissociation of molecular hydrogen. The molecular adsorption energies $\delta E^{mol}$ in Table I, particularly the ones for the four-atom chain, clearly show the enhanced chemical reactivity of the low-coordination Au atoms, which gives the dissociation process on the Au nanowire an exothermic character that is more pronounced for the longer chains. The presence of more than one H atom can, in certain cases, significantly modify the conductance. While the chain with three Au atoms and two H atoms (case 2-2H in Fig. 6) presents a conductance of $0.45G_0$ (similar to the one H atom case), for a four-Au-atom nanowire (Fig. 7) the conductance takes values around $0.1-0.2G_0$, depending on the particular adsorption configuration.

The very different influence in the conductance upon adsorption of molecular or atomic hydrogen can be understood in terms of the changes induced in the LDOS. Figure 4 illustrates these changes for the case of the four-atom chain, comparing the LDOS for the different atoms in the clean wire with the results for the relaxed configurations found upon adsorption of a $H_2$ molecule or a single H atom. In the case of molecular hydrogen, the LDOS shows a well-localized molecular bonding state of hydrogen around 7.3 eV below the Fermi level. There is very little resonance in the LDOS of

TABLE I. Molecular $\delta E^{mol}$ adsorption energies calculated using the FIREBALL method with the LDA approximation for the exchange-correlation functional. The adsorption energies are defined as $\delta E^{mol}=(E^{ads}-E^{clean})-0.5nE^{H_2}$, where $n$ is the number of hydrogen atoms and $E^{H_2}=-30.16$ eV corresponds to the hydrogen molecule calculated with the same method. The different labels correspond to the structures shown in Figs. 5–7.

| Structure | 1-H2 | 1-H | 2-H2 | 2-Ha | 2-Hb | 2-2H | 3-H2 | 3-Ha | 3-Hb | 3-Hc | 3-2Ha | 3-2Hb | 3-2Hc |
|---|---|---|---|---|---|---|---|---|---|---|---|---|---|
| $\delta E^{mol}$ | −0.27 | −0.30 | −0.38 | −0.57 | −0.58 | −1.05 | −0.41 | −0.65 | −0.98 | −0.60 | −1.80 | −1.37 | −1.60 |

the nearest gold atoms that can be localized at the energies corresponding to the molecular bonding state. This is consistent with the weak interaction of the $H_2$ molecule with the gold chain, as reflected in the small adsorption energy. More importantly, the density of states of the nearest gold atoms remains practically unchanged with respect to the clean chain, particularly in the energy range close to the Fermi level, which explains the absence of a significant change in the conductance. On the other hand, the adsorption of atomic hydrogen induces dramatic changes in the LDOS of the nearest Au atoms. The strong interactions is reflected in (1) the strong hybridization between the hydrogen bonding state and *s* orbital gold states at −7.3 eV below the Fermi level and (2) the significant change in the width and mean position of the Au *d* states, which move toward larger binding energies. This is particularly clear in the case of the central atom in the chain that is bonded to H (the atom labeled Au4 in Fig. 4). The significant reduction in the conductance, which provides an explanation for the fractional peak around $0.6G_0$ found in the experiments, can then be mainly attributed to the reduction in the DOS at the Fermi level of the Au atoms bonded to H, as emphasized in Fig. 8.

Both the conductance and the total energy results, discussed so far, support the dissociation of molecular hydrogen on the Au monoatomic chains. As the energetics were discussed in terms of the local-orbital code, using the LDA approximation for the exchange correlation, we reanalyzed the dissociation mechanism on freely suspended Au wires, with H (or $H_2$) adsorbed on them, using CASTEP (Refs. 46 and 47), with a gradient corrected approximation[45] (GGA) for the exchange-correlation functional. This simplified model for the nanowire was dictated by the computational resources needed for this full calculation, but it offers the possibility to discuss the relative contribution of the low dimensionality and the strain in the enhanced reactivity of the nanowire. This analysis (described in detail in Ref. 41) has unveiled an optimal dissociation path for $H_2$ with an activation barrier around 0.10 eV, which can be easily overcome even at the low temperatures considered in the experiments. It is important to note that such a low-activation barrier has been found for the case where the nanowire is submitted to a tensile strain around 11% with respect to the equilibrium position. Our calculations for the unstrained wire show quite large barriers (≈0.5 eV) for the dissociation. These results point out again the fundamental role of the strain on the chemical reactivity of the gold chains, which can be simply explained in terms of the shift toward the Fermi level and the narrowing of the Au *d* bands.

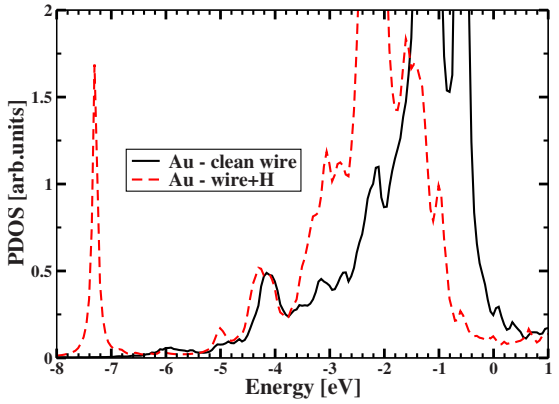


FIG. 8. (Color online) LDOS for a typical Au atom on a pure monoatomic chain (solid line) and a Au atom interacting with the adsorbed *H*. The energy scale is shifted to place Fermi level $E_F$ at value 0.0.

## V. INTERACTION OF ATOMIC OXYGEN WITH THE Au NANOCONTACTS

In this section, we discuss the role of atomic oxygen in the formation of monoatomic chains and their stability. Our approach is different from the one followed for hydrogen, as we want to address, from a theoretical perspective, the enhancement in chain formation seen in the experiments and its relation with the possible incorporation of oxygen into the metal chain. On the other hand, based on our study for H, we can expect $O_2$ to react strongly, and we will present some theoretical results supporting this point of view at the end of this section. Accordingly, we have simulated the whole stretching process in the presence of atomic oxygen. We have started from the same initial configuration we have considered for the clean Au wire. Then, we have added an O atom in the middle of the wire and let the system relax to the ground state configuration [see Fig. 9(a)]. From this point on, we follow the same protocol described for the clean wire to simulate the nanowire formation under strain.

From Fig. 10, where the total energy versus displacement is shown for both the clean and contaminated wire, it is evident that the presence of oxygen changes the character of the deformation process. While the clean wire shows well-defined jumps at the plastic stages, where the incorporation of new atoms to the chain takes place, the energy curves for the contaminated nanowire show a more continuous evolution, except for the last incorporation of a Au atom to the chain (G to H) in the contaminated case, which actually involves the detachment of the O atom from one of the electrodes. The ability of atomic oxygen to enhance the chain formation, in good agreement with the experimental

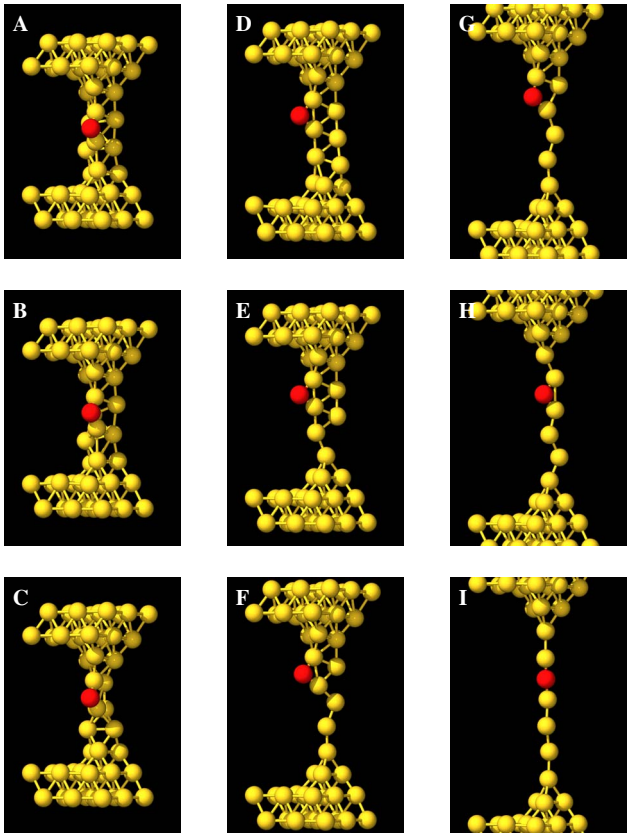


FIG. 9. (Color online) Ball-and-stick structure models for different snapshots of the DFT-LDA simulation using the FIREBALL code for the stretching of a gold nanocontact in the presence of atomic oxygen impurity, showing the incorporation of the oxygen atom and the formation of a monoatomic chain longer than in the pure Au case.

evidence,[40] is clear as we are able to form a longer atomic chain including six Au atoms and the O atom that is incorporated during the final elastic stage before the final breaking of the wire. The average Au-O and Au-Au bond lengths are around 1.95 and 2.6 Å, respectively.

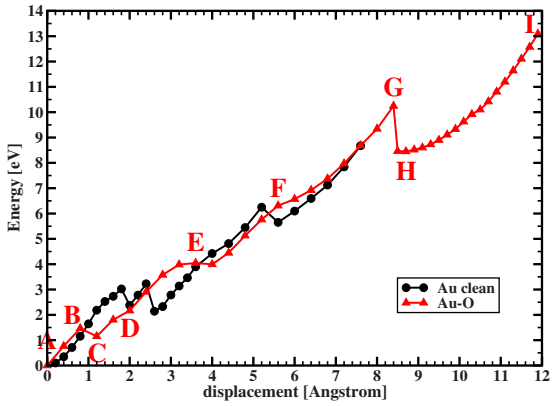


FIG. 10. (Color online) Total energy per unit cell (in eV) along the stretching path for the clean Au nanowire and for a Au nanowire with atomic oxygen impurity. The reference for each case is the energy of the initial relaxed configuration.

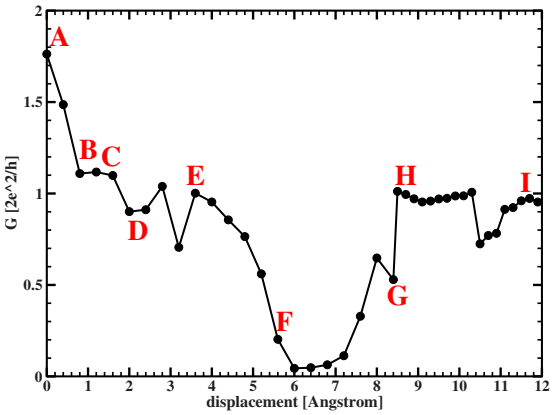


FIG. 11. (Color online) Total differential conductance for the Au nanowire with atomic oxygen impurity along the deformation process (with labels similar to tubse in Fig. 10).

We now address in more detail the deformation process of the Au nanocontact with atomic oxygen along the stretching path. Figure 9 illustrates the relevant configurations. At the initial step, frame A, the oxygen atom is bonded with their two nearest Au atoms, forming a local configuration that remains stable until frame G, where the oxygen atom starts to be incorporated into the atomic chain. From the subsequent snapshots, it is evident that the nature of the deformation is quite different from the clean nanocontact, where the monoatomic constriction is created. Here, we first observe the formation of a planar structure defined by two parallel monoatomic chains [see Fig. 9(b)–9(d)]. Afterward, the atomic constriction is formed (frame E) next to the position where the oxygen is adsorbed, indicating that the oxygen makes stronger the Au bonds in its local environment. At frame G, the oxygen starts to be incorporated into the chain during an elastic deformation stage that leads to the final breaking of the chain. The presence of atomic oxygen gently reduces the Au-Au bond by 0.1 Å, compared to the typical Au-Au distance in the clean nanocontact. We find values for the Au-O bond distance around 1.94 Å, in good agreement with the experimental values extracted from the peaks in the distance histograms.[40] Both Au-Au and Au-O distances gradually increase by ~10% along the deformation path. The analysis of the total charge densities (see Fig. 12) for selected atomic configurations confirms the strength of the Au-O bond at the different stages of the stretching path. This enhanced bonding between Au and O (compared to the Au-Au bond) is illustrated with an isosurface corresponding to a large value of the charge density (0.5 $e/\mathrm{A}^3$) such that, while the Au atoms appear disconnected, there is a clear evidence of charge pileup along the direction of the Au-O bonds. This effect is present since the early stages of the deformation process and becomes even more apparent as we further increase the applied tensile stress and as the atomic oxygen is incorporated into the chain. The strength of the Au-O bonds can be at the origin of the large mechanical stability of gold monoatomic chains in the presence of oxygen impurities found in the experiments.

The transport properties of the nanocontact in the presence of atomic oxygen along the stretching process are illus-

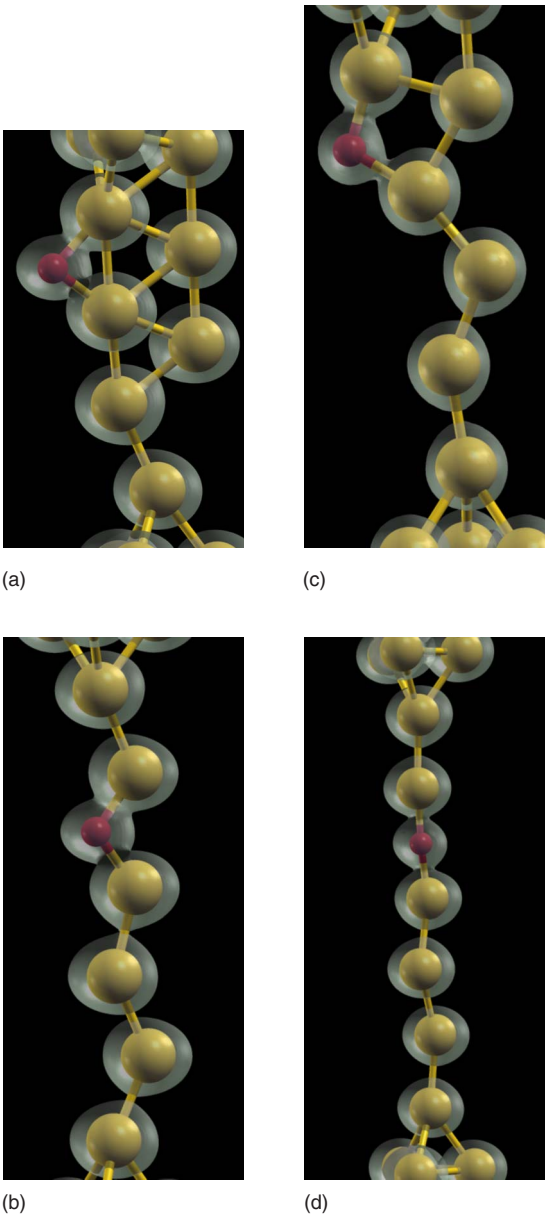


FIG. 12. (Color online) Isosurfaces of total charge electronic density (corresponding to the value 0.5 $e/\text{Å}^3$) for the Au nanocontact with atomic oxygen impurity at different steps of the chain formation process (cases F–I in Fig. 12, corresponding to stretching displacements of 3.6, 6.0, 8.5, and 10.7 Å, respectively).

trated in Fig. 11. The conductance rapidly evolves toward values close to the conductance quantum as the strain is increased and shows a significant drop between the E and H frames, just as the local configuration O-$Au_2$ is deformed. Once the oxygen is incorporated into the monoatomic chain (frame H), the conductance recovers the value near $1G_0$. From our analysis of the LDOS, we conclude that at variance with the H case, the dramatic reduction in the conductance is not only due to the partial decrease of the *s*-orbital DOS at the Fermi level on the gold atoms (shown in Fig. 13) but also results from the interplay between this decrease and interference effects among the Au atoms close to the oxygen. The variation of the conductance during the deformation process

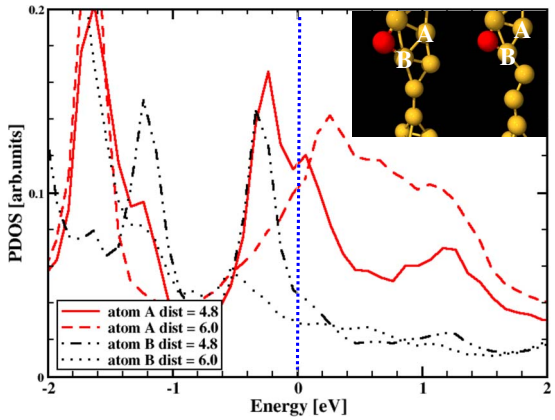


FIG. 13. (Color online) Local density of states, projected on the *s* orbitals, around the Fermi level (placed at $E=0.0$, blue line) for the two Au atoms marked on the inset. Continuous (dashed) curves correspond to a stretching displacement of 4.8 (6.0) Å.

shown in Fig. 12 does not certainly coincide with the individual breaking traces shown in the published experimental data,[40] where the conductance seems to be close to $1G_0$ during the whole process. However, the structures between E and H and, particularly, the very low conductance stages between F and G—where the oxygen atom is detached from the electrode—are consistent with the large peak around $G \approx 0$ and the quite broad $G \approx G_0$ peak found in the conductance histograms recorded in the presence of oxygen (see Fig. 2 in Ref. 40).

The analysis above shows that we can understand some of the basic experimental features, assuming the presence of atomic oxygen during the breaking process. This leads us back to the problem of the dissociation of the molecular oxygen that is introduced into the vacuum chamber. In order to study the energetics of the dissociation process for an $O_2$ molecule on a monoatomic gold chain, we have performed an analysis similar to the one described above for the $H_2$ molecule, exploring the dissociation path on an ideal infinite chain with DFT-PW-GGA calculations using CASTEP.[46] The results shown in Table II correspond to the adsorption on a Au chain subject to an 11% strain, where we have found low barriers for $H_2$ dissociation. We have also included a similar study with local-orbital LDA calculations as implemented in FIREBALL in order to show that the main conclusions extracted from the LDA analysis of the whole deformation process presented above, although affected by the systematic overbinding associated with LDA, are robust. Focusing on the more accurate GGA energetic results, we have found a very weak attractive interaction, $\sim -0.04$ eV, between $O_2$ and the infinite ideal Au wire. On the other hand, the system with atomic oxygen embodies a strong chemical interaction between atomic oxygen and the gold wire [with $\delta E^{mol}(2O) = -2.12$ eV], which is accompanied by significant structural changes in the Au chain. These energies are very similar to the ones found for hydrogen and provide a sound basis for the possible dissociation of molecular oxygen. Finally, we have performed an extensive search for the dissociation path of the $O_2$ molecule on the infinite chain. At variance with the H case, we have not found a low-activation energy path even

TABLE II. Adsorption energies for atomic and molecular oxygen on a Au chain with an 11% strain calculated using both the FIREBALL method with the LDA approximation for the exchange-correlation functional and the plane-wave code CASTEP with the GGA approximation. The adsorption energies are defined as $\delta E^{mol}=(E^{ads}-E^{clean})-E^{O_2}$, where $E^{O_2}$ corresponds to the molecular oxygen energy.

| | $O_2$ (eV) | $\delta E^{mol}(O_2)$ (eV) | $\delta E^{mol}(2O)$ (eV) |
|---|---|---|---|
| CASTEP GGA | −10.00 | −0.04 | −2.12 |
| FIREBALL LDA | −9.80 | −0.34 | −3.00 |

for the strained systems (up to the maximum strain sustained by the clean chain): In all the cases, we have obtained quite large minimal dissociation barriers, near 2 eV, similar to those reported in a previous study.[26] The enhanced reactivity of Au clusters has been attributed in the literature to both the lower coordination (compared to bulk and surface structures) favored by the open cluster structures and to charging effects that involve the material that hosts the clusters. Our results show that even in the ultimate limit of a 1D chain, the first mechanism seems not enough to favor significantly the dissociation of molecular oxygen. At this stage, one can only speculate with possible "local" charging effects associated with the current flowing through the nanowire during the experiment as an additional factor enhancing its reactivity. This is a complicated, dynamical effect, and its treatment is beyond the scope of this work. It remains an open problem for future research.

## VI. CONCLUSIONS

In conclusion, we have performed an *ab initio* study of the evolution of the mechanical and transport properties of clean and contaminated Au nanowires along the deformation path. In spite of the limited number of initial configurations that can be explored with *ab initio* methods, this methodology, where no assumptions are made about the final contact structure, provides relevant information about the structural and transport properties of gold nanocontacts and about how they are affected by intentional contamination. In particular, we have provided significant insight into the changes in the atomic relaxation mechanisms of gold nanocontacts in the presence of atomic impurities (such as H and O) during the breaking process. The simulations have shown how atomic oxygen enhances the chain formation process, allowing the system to extract more atoms from the electrodes and, finally, incorporating itself into the monoatomic chain. The mechanisms revealed by the simulations, such as the reinforcement of the Au bonds in the contacts due to the presence of oxygen that changes the character of the deformation process compared to the clean wire, are robust. From this perspective, we believe that our work can be used as a benchmark to test faster classical interatomic potential approaches suitable for a full statistical analysis of the process.

The detailed analysis of the LDOS for selected nanowire configurations, including the cases with hydrogen impurities, allows us to understand the direct connection between the enhanced chemical reactivity of gold atoms and both the low coordination and the applied tensile stress. These two effects cooperate to produce the displacement of the *d*-orbital bands toward the Fermi level (compared to the bulk case), which is ultimately responsible for the enhanced reactivity. In addition, we have calculated the conductance for the optimized structures of the clean and contaminated nanocontacts along the deformation path. In both the hydrogen oxygen cases, the presence of adsorbed atomic impurities introduces significant changes in the conductance, providing a quantitative explanation for the new peaks found in the conductance histograms recorded in the presence of the corresponding molecular species.[38–40] The exothermic character of the dissociation process in the nanowire found in our study–which is related to the enhanced reactivity of these strained, quasi-1D systems–provides a sound basis for the presence of these atomic impurities, although the problem of finding a low-activation energy path for the molecular oxygen remains open.

## ACKNOWLEDGMENTS

We acknowledge useful discussions with W. H. Thijssen and J. van Ruitenbeek. This work has been supported by the DGI-MCyT (Spain) under Contracts No. MAT2004-01271, No. MAT2005-01298, and No. NAN2004-09183-C10-07 and by Comunidad de Madrid under Contract No. 0505/MAT-0303. The work of P.J. has been supported by the MSMT under Grant No. 1K05020, the Institutional Research Plan No. AV0Z10100521, and GAAV under Grants No. IAA100100616, No. KAN400100701 and No. IAA1010413. Part of these calculations have been performed in the MareNostrum supercomputer at the BSC-CNS.

[1] N. Agräit, A. Levy-Yeyati, and J. van Ruitenbeek, Phys. Rep. **377**, 81 (2003).
[2] G. Rubio, N. Agräit, and S. Vieira, Phys. Rev. Lett. **76**, 2302 (1996).
[3] E. Scheer, P. Joyez, D. Esteve, C. Urbina, and M. H. Devoret, Phys. Rev. Lett. **78**, 3535 (1997).
[4] E. Scheer, N. Agrait, J. C. Cuevas, A. Levy Yeyati, B. Ludoph, A. Martín-Rodero, G. R. Bollinger, J. M. van Ruitenbeek, and C. Urbina, Nature (London) **394**, 154 (1998).
[5] G. Rubio-Bollinger, S. R. Bahn, N. Agrait, K. W. Jacobsen, and S. Vieira, Phys. Rev. Lett. **87**, 026101 (2001).
[6] U. Landman, W. D. Luedtke, B. E. Salisbury, and R. L. Whetten, Phys. Rev. Lett. **77**, 1362 (1996).
[7] T. N. Todorov and A. P. Sutton, Phys. Rev. Lett. **70**, 2138 (1993).
[8] A. M. Bratkovsky, A. P. Sutton, and T. N. Todorov, Phys. Rev. B **52**, 5036 (1995).
[9] M. R. Sörensen, M. Brandbyge, and K. W. Jacobsen, Phys. Rev. B **57**, 3283 (1998).
[10] A. Nakamura, M. Brandbyge, L. B. Hansen, and K. W. Jacobsen, Phys. Rev. Lett. **82**, 1538 (1999).
[11] N. D. Lang, Phys. Rev. B **52**, 5335 (1995).
[12] C. C. Wan, J.-L. Mozos, G. Taraschi, J. Wang, and H. Guo, Appl. Phys. Lett. **71**, 419 (1997).
[13] N. Kobayashi, M. Brandbyge, and M. Tsukada, Phys. Rev. B **62**, 8430 (2000).
[14] N. Kobayashi, M. Brandbyge, and M. Tsukada, Surf. Sci. **433-435**, 854 (1999).
[15] H. Mehrez, A. Wlasenko, B. Larade, J. Taylor, P. Grutter, and H. Guo, Phys. Rev. B **65**, 195419 (2002).
[16] M. Brandbyge, J.-L. Mozos, P. Ordejon, J. Taylor, and K. Stokbro, Phys. Rev. B **65**, 165401 (2002).
[17] J. J. Palacios, A. J. Perez-Jimenez, E. Louis, E. San Fabian, and J. A. Verges, Phys. Rev. B **66**, 035322 (2002).
[18] P. Jelinek, R. Pérez, J. Ortega, and F. Flores, Phys. Rev. B **68**, 085403 (2003).
[19] P. Jelinek, R. Pérez, J. Ortega, and F. Flores, Surf. Sci. **566-568**, 13 (2004).
[20] P. Jelinek, R. Pérez, J. Ortega, and F. Flores, Nanotechnology **16**, 1023 (2005).
[21] J. P. Lewis, K. R. Glaesemann, G. A. Voth, J. Fritsch, A. A. Demkov, J. Ortega, and O. F. Sankey, Phys. Rev. B **64**, 195103 (2001).
[22] P. Jelinek, H. Wang, J. P. Lewis, O. F. Sankey, and J. Ortega, Phys. Rev. B **71**, 235101 (2005).
[23] N. Mingo, L. Jurczyszyn, F. J. Garcia-Vidal, R. Saiz-Pardo, P. L. de Andres, F. Flores, S. Y. Wu, and W. More, Phys. Rev. B **54**, 2225 (1996).
[24] A. I. Yanson, G. R. Bollinger, H. E. van den Brom, N. Agrait, and J. M. van Ruitenbeek, Nature (London) **395**, 783 (1998).
[25] S. B. Legoas, D. S. Galvao, V. Rodrigues, and D. Ugarte, Phys. Rev. Lett. **88**, 076105 (2002).
[26] S. R. Bahn, N. Lopez, J. K. Norskov, and K. W. Jacobsen, Phys. Rev. B **66**, 081405(R) (2002).
[27] F. D. Novaes, A. J. R. da Silva, E. Z. da Silva, and A. Fazzio, Phys. Rev. Lett. **90**, 036101 (2003).
[28] N. V. Skorodumova and S. I. Simak, Phys. Rev. B **67**, 121404(R) (2003).
[29] R. N. Barnett, H. Häkkinen, A. G. Scherbakov, and U. Landman, Nano Lett. **4**, 1845 (2004).
[30] F. D. Novaes, A. J. R. da Silva, E. Z. da Silva, and A. Fazzio, Phys. Rev. Lett. **96**, 016104 (2006).
[31] N. V. Skorodumova, S. I. Simak, A. E. Kochetov, and B. Johansson, Phys. Rev. B **75**, 235440 (2007).
[32] E. Anglada, J. A. Torres, F. Yndurain, and J. M. Soler, Phys. Rev. Lett. **98**, 096102 (2007).
[33] H. Ohnishi, Y. Kondo, and K. Takayanagi, Nature (London) **395**, 780 (1998).
[34] H. Häkkinen, R. N. Barnett, and U. Landman, J. Phys. Chem. B **103**, 8814 (1999).
[35] J. A. Torres, E. Tosatti, A. Dal Corso, F. Ercolessi, J. J. Kohanoff, F. D. Di Tolla, and J. M. Soler, Surf. Sci. **426**, L441 (1999).
[36] E. Z. da Silva, A. J. R. da Silva, and A. Fazzio, Phys. Rev. Lett. **87**, 256102 (2001).
[37] C. Untiedt, A. I. Yanson, R. Grande, G. Rubio-Bollinger, N. Agrait, S. Vieita, and J. M. van Ruitenbeek, Phys. Rev. B **66**, 085418 (2002).
[38] Sz. Csonka, A. Halbritter, G. Mihaly, E. Jurdik, O. I. Shklyarevskii, S. Speller, and H. van Kempen, Phys. Rev. Lett. **90**, 116803 (2003).
[39] Sz. Csonka, A. Halbritter, and G. Mihály, Phys. Rev. B **73**, 075405 (2006).
[40] W. H. A. Thijssen, D. Marjenburgh, R. H. Bremmer, and J. M. van Ruitenbeek, Phys. Rev. Lett. **96**, 026806 (2006).
[41] P. Jelinek, R. Pérez, J. Ortega, and F. Flores, Phys. Rev. Lett. **96**, 046803 (2006).
[42] D. Krüger, H. Fuchs, R. Rousseau, D. Marx, and M. Parrinello, Phys. Rev. Lett. **89**, 186402 (2002).
[43] M. A. Basanta, Y. J. Dappe, P. Jelinek, and J. Ortega, Comput. Mater. Sci. **39**, 759 (2007).
[44] O. F. Sankey and D. J. Niklewski, Phys. Rev. B **40**, 3979 (1989).
[45] J. P. Perdew, J. A. Chevary, S. H. Vosko, K. A. Jackson, M. R. Pederson, D. J. Singh, and C. Fiolhais, Phys. Rev. B **46**, 6671 (1992).
[46] M. D. Segall, P. J. D. Lindan, M. J. Probert, C. J. Pickard, P. J. Hasnip, S. J. Clark, and M. C. Payne, J. Phys.: Condens. Matter **14**, 2717 (2002).
[47] Au, H, and O atoms are described with ultrasoft pseudopotentials (Ref. 48) and wave functions expanded with a PW cutoff of 340 eV.
[48] D. Vanderbilt, Phys. Rev. B **41**, 7892 (1990).
[49] G. Taraschi, J.-L. Mozos, C. C. Wan, H. Guo, and J. Wang, Phys. Rev. B **58**, 13138 (1998).
[50] J. Heurich, J. C. Cuevas, W. Wenzel, and G. Schön, Phys. Rev. Lett. **88**, 256803 (2002).
[51] D. Sánchez-Portal, E. Artache, J. Junquera, P. Ordejon, A. Garcia, and J. M. Soler, Phys. Rev. Lett. **83**, 3884 (1999).
[52] E. Z. da Silva, F. D. Novaes, A. J. R. da Silva, and A. Fazzio, Phys. Rev. B **69**, 115411 (2004).
[53] R. H. M. Smit, C. Untiedt, G. Rubio-Bollinger, R. C. Segers, and J. M. van Ruitenbeek, Phys. Rev. Lett. **91**, 076805 (2003).
[54] A. Grigoriev, N. V. Skorodumova, S. I. Simak, G. Wendin, B. Johansson, and R. Ahuja, Phys. Rev. Lett. **97**, 236807 (2006).
[55] P. Pernas, E. Anda, and F. Flores, J. Phys. C **4**, 5309 (1992).
[56] Y. J. Lee, M. Brandbyge, M. J. Puska, J. Taylor, K. Stokbro, and R. M. Nieminen, Phys. Rev. B **69**, 125409 (2004).
[57] H. S. Sim, H. W. Lee, and K. J. Chang, Phys. Rev. Lett. **87**, 096803 (2001).